*Technical Report No. 32-561*

# *An Experimental Investigation of Uncooled Thrust Chamber Materials for Use in Storable Liquid Propellant Rocket Engines*

*R. W. Rowley*

D. R. Bartz, Chief
*Propulsion Research Section*

JET PROPULSION LABORATORY
CALIFORNIA INSTITUTE OF TECHNOLOGY
PASADENA, CALIFORNIA

February 15, 1964

Prepared Under Contract No. NAS 7-100
National Aeronautics & Space Administration

# CONTENTS



# TABLES

# FIGURES

## ABSTRACT

17820 A

An experimental investigation of the comparative merits of various uncooled thrust chamber materials was conducted by performing engine tests in which $N_2O_4/N_2H_4$ propellants were used at a nominal mixture ratio of 1.0. The chamber pressure was 150 psia and the nominal sea-level thrust was 85 lb. Erosion of graphites, ablative plastics, and refractory metals was found to be a function of the local thermal and chemical environments existing at the thrust chamber wall. The role of a particular impinging-stream injector in influencing local conditions at the wall was determined by (1) evaluating the properties of the spray produced by nonreacting liquids and (2) measuring local heat-transfer rates to the chamber wall in the operating rocket engine by means of embedded thermocouples and a transient conduction analysis. Local erosion of Refrasil–phenolic, pyrolytic graphite, and ZT graphite nozzle throats tested with this injector was found to be qualitatively related to these local gas-side boundary conditions.

Author


## I. INTRODUCTION

The exploration of space provides numerous applications for low-thrust chemical propulsion systems for such purposes as attitude control, midcourse trajectory correction, and terminal maneuvering of spacecraft. Propulsion systems using high-energy liquid bipropellants or a high-energy monopropellant appear to be well suited to these applications, provided that such systems can be made to operate simply and reliably. However, the accomplishment of many mission objectives will require that the rocket engines be throttlable and/or restartable. The combination of these three requirements (i.e., low thrust level, high-energy propellants, and variable propellant flow rate) imposes severe limitations on regenerative-cooling capabilities, and the use of other thrust chamber cooling techniques is indicated. Two such methods which appear promising are ablation cooling and radiation cooling. This Report summarizes the results obtained in an experimental investigation of the suitability of some of the thrust chamber materials adaptable to these two techniques. In this study, the relative performance of the several materials was determined by rocket engine tests in which the candidate material formed either the nozzle or the complete thrust chamber. Aside from the obvious advantage of subjecting the materials to the actual en-

vironment of interest, rather than a "simulated" environment as produced by a torch or plasma jet, the use of rocket engine tests for materials evaluation provides considerable experience in fabricating materials in the complicated shapes required for nozzles and thrust chambers. This experience would be invaluable in any actual development effort.

Most of the tests were conducted with the storable propellant combination nitrogen tetroxide ($N_2O_4$) and hydrazine ($N_2H_4$), used at a mixture ratio of 1.0. However, this phase of the study was supplemented by a cursory investigation of the effects of a different chemical environment on ablative materials, in which chlorine trifluoride ($ClF_3$) and hydrazine propellants were used at a mixture ratio of 2.2. Nominal chamber pressure was 150 psia with both propellant combinations. A sea-level thrust of 85 lb was chosen as representative of the applications of interest, and a test duration of 300 sec was considered a representative maximum thrusting time. The configuration of the test engines is summarized in Table 1 and, unless otherwise noted, all tests covered by this Report were conducted with thrust chambers fabricated to such dimensions.

**Table 1. Engine configuration**

| | |
|---|---|
| Combustion chamber length | 5.2 in.[a] |
| Combustion chamber diameter | 2.0 in. |
| Throat diameter | 0.75 in. |
| Contraction ratio | 7.1 |
| Characteristic chamber length $L^*$ | 42 in.[a] |

[a]Three tests of ablative thrust chambers with a length of 3.8 in. and an $L^*$ of 30 in. were conducted (see Table 4).

Materials to be tested were selected on the basis of their anticipated resistance to the rocket engine environment and their applicability to light, simple (and, hence, potentially reliable) thrust chamber design. Three types of materials were tested:

1. Ablative materials
2. Graphites
3. Refractory metals

# II. MATERIALS TESTED

## A. Ablative Materials

Ablation may be described as cooling by means of sacrificial mass transfer, wherein a portion of the heated wall is allowed to melt and/or vaporize, thus maintaining the surface at a temperature below the temperature which the wall would reach without cooling. Several mechanisms interact to produce the desired result:

1. Heat is absorbed in raising the temperature of the ablative material to the melting or vaporization temperature.
2. Heat is absorbed in changing the phase of the ablative material (melting and/or vaporization) and in endothermic reactions (such as the cracking of long-chain hydrocarbons in the production of a char from phenolic resins).
3. Gases, injected into the boundary layer as the ablative material vaporizes, reduce the heat transferred from the free stream to the wall by increasing the thickness of the boundary layer.

The rates at which these processes occur determine the rate at which material is removed from the heated surface: i.e., the *ablation rate*. In the case of the ablators which form a char, such as reinforced plastics, several specific terms have become associated with various modes of material behavior. When the surface recedes at the same rate at which the char advances into the virgin material, the process is termed *steady-state* ablation. If the char depth grows with time (i.e., the surface recedes at a slower rate than the rate at which the char proceeds through the wall) the process is called *transient* ablation. A limiting case of transient ablation, occurring when the surface does not recede at all, has been called *charring* ablation.

Reinforced plastics have generally demonstrated performance superior to that of homogeneous plastics and ceramics as ablators in liquid and solid rocket engine nozzles, and the present investigation was limited to such heterogeneous materials. Several types of reinforced plastics were tested, with primary emphasis placed on the combination of Refrasil[1] fiber reinforcement and phenolic resin binder. To some extent, the evaluation of these various ablative materials paralleled similar investigations conducted in the solid propellant rocket nozzle field and provided comparative information on the effects of the differing environments on material performance.

Several tests were conducted using thrust chambers fabricated from Refrasil–phenolic material (approximately 30% resin by weight), as shown in Fig. 1(a). The nozzle section was a high-pressure laminate using Refrasil cloth in "edgegrain" fashion, oriented 90 deg to the nozzle axis. Combustion chamber sections employing this 90-deg

[1]Trade name of material supplied by H. I. Thompson Fiber Glass Co., Los Angeles, California.

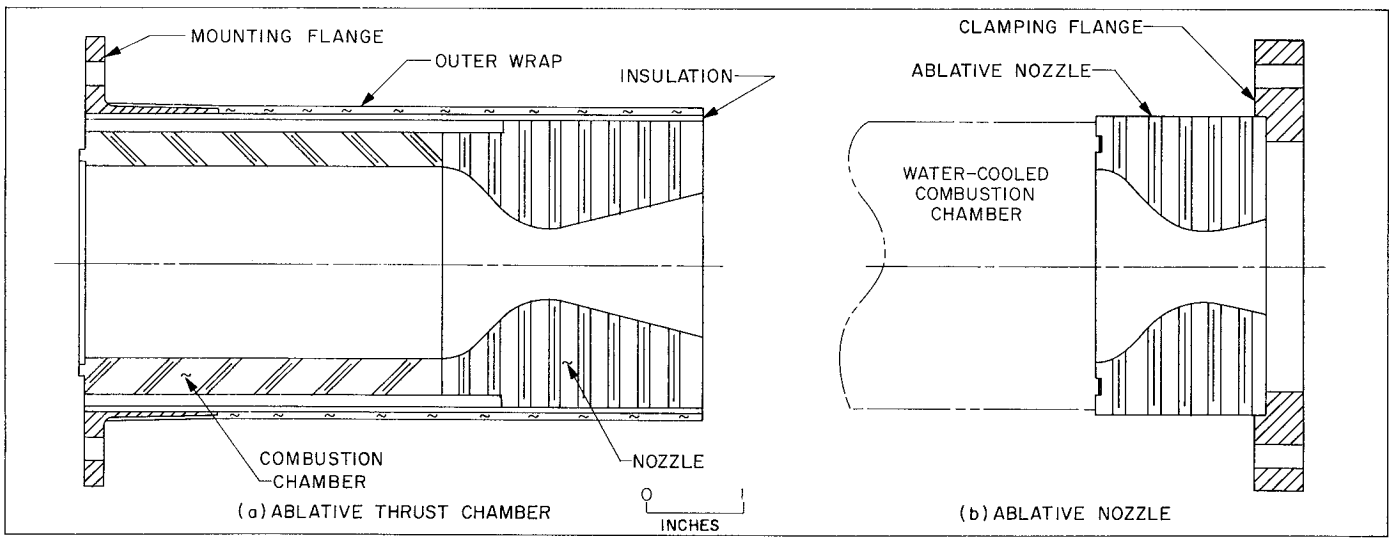


**Fig. 1. Configuration of ablative thrust chamber and nozzle**

orientation, and also a 45-deg-trailing-angle construction, were tested. An outer wrap of glass rovings was provided to contain the pressure forces, with flat wrappings of Refrasil tape between the ablative liner and the rovings to provide insulation for protection of the outer wrap. The ablative liner was 0.375 in. thick in the combustion chamber, and the entire thrust chamber weighed 3.0 lb, including the steel flange. The characteristic chamber length $L^*$ of the unit was 30 in.; however, a water-cooled adapter was used in some tests to increase the chamber length and provide an $L^*$ of 42 in.

In order to evaluate the relative erosion resistance of various commercially available ablative plastics, moldings of the materials of interest were machined into the form of nozzles, as shown in Fig. 1(b), which were clamped to a water-cooled combustion chamber for testing. These materials included Refrasil–phenolic in various orientations, as well as several other reinforced plastics under consideration for use in solid rocket motor nozzles, such as asbestos, zirconium oxide, and graphite and carbon cloths, all with phenolic resin binders. No outer wrap was needed, since the nozzles were relatively thick, and the uncharred material provided sufficient strength.

### B. Graphites

Probably the most interesting materials available for potential use in liquid rocket engine thrust chambers are pyrolytic graphite and related pyrolytically deposited alloys and compounds. Pyrolytic graphite is produced by depositing on a mandrel, at high temperature, the carbon resulting from the decomposition of a hydrocarbon gas such as methane. The pyrolytic material differs from ordinary graphite in that the crystallites are highly oriented, resulting in thermal and mechanical properties which are considerably more anisotropic than the properties of conventional graphite. The strength–weight ratio of pyrolytic graphite at high temperatures is exceptional and offers the possibility of fabricating very light thrust chambers of the thin-wall freestanding type. A disadvantage is the brittle nature of the material at temperatures below 4500°F (Ref. 1).

The two configurations of pyrolytic graphite nozzles and thrust chambers tested are illustrated in Fig. 2. Initial tests were conducted with the graphite-backed nozzles shown in Fig. 2(a); in these tests, the pyrolytic shell remained attached to the female mandrel, this concept representing an early stage in the development of pyrolytic graphite components, and the nozzles were clamped to a water-cooled combustion chamber. Later tests were conducted with the freestanding thrust chamber shown in Fig. 2(b), where the substrate used during deposition was removed. This represented a later "state of the art" and approached a flyable design. Although the internal dimensions of this unit were roughly the same as those of thrust chambers used in testing other materials, the radius at the entrance to the converging portion of the nozzle and the radius at the injector attachment flange were made relatively large to reduce residual thermal stresses introduced during the fabrication process. Thickness of the pyrolytic graphite was approximately 0.050 in. (varying from 0.040 to 0.060 in.) and, as a result, the thrust chamber weighed only 0.2 lb.

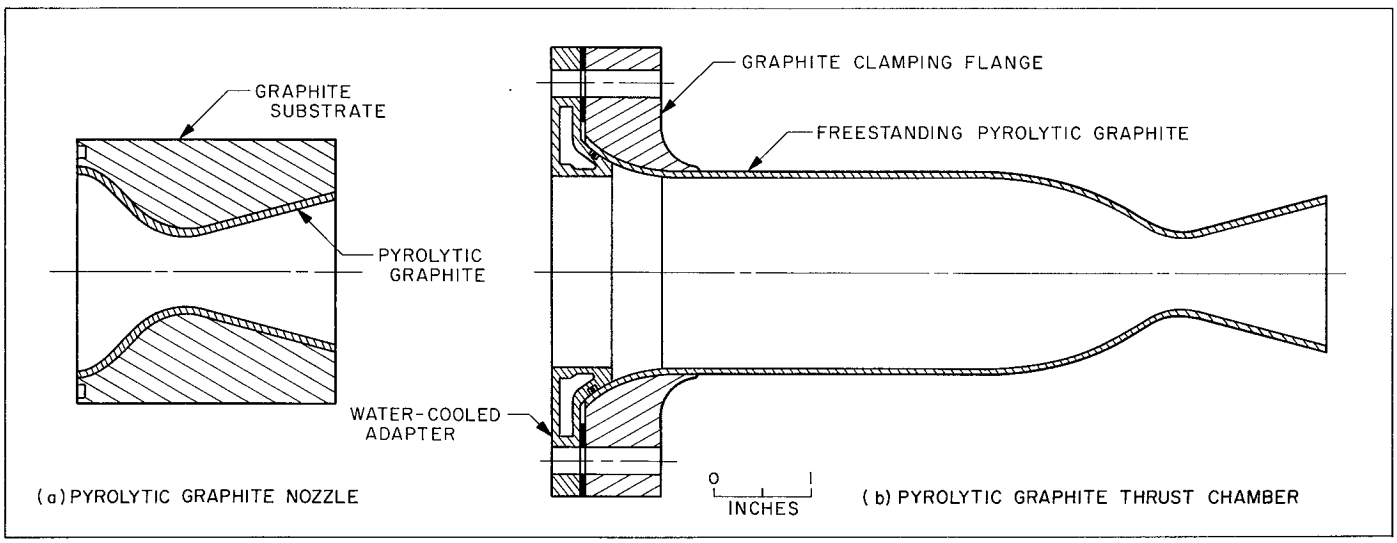


**Fig. 2. Configuration of pyrolytic graphite thrust chamber and nozzle**

In order to compare the erosion rates of pyrolytic graphite with the performance of other types of graphite, tests of two types of high-quality normal graphite were conducted. One type was a commonly used high-density graphite, ATJ (density, 1.73 gm/cc). The second, designated as ZT (density, 1.94 gm/cc), has demonstrated better erosion resistance than ATJ in some solid rocket motor nozzle applications. The configuration of the nozzles tested was similar to that of the graphite-backed pyrolytic graphite nozzles, except that the entire nozzle was ordinary graphite.

### C. *Refractory Metals*

Like pyrolytic graphite, refractory metals offer the possibility of fabricating thin-wall radiation-cooled thrust chambers. Particularly interesting materials in this class are tungsten and alloys of tantalum and tungsten. Tungsten possesses good high-temperature strength and has been used successfully in aluminized solid propellant rocket motor nozzles; however, it is a brittle material and is difficult to fabricate at room temperature. Care is required in designing tungsten components to ensure against stresses (particularly thermally induced stresses) which cannot be relieved by local yielding at temperatures below the brittle–ductile transition point. For wrought tungsten, this transition temperature is approximately 700°F. The 90% tantalum–10% tungsten alloy also has good high-temperature strength and, since it is ductile, is easier to fabricate than tungsten. Both of these metals have the disadvantage of high densities; in small thrust chambers, however, the weight is comparable to that of ablative engines.

Nozzles of pure tungsten and 90Ta–10W alloy were fabricated to evaluate the comparative merits of these metals. As shown in Fig. 3, the nozzles were formed from three pieces joined by welding. The contour portions were die-formed to a thickness of approximately 0.090 in. and welded to a flange, which had been machined from hot-pressed material. The gasket groove was machined after welding, and the welds were ground smooth by hand, but the internal contour was not otherwise machined. The completed 90Ta–10W alloy nozzles weighed 1.0 lb; the tungsten nozzles weighed 1.1 lb. These nozzles were clamped to a water-cooled combustion chamber for testing.

After initial tests with one tungsten nozzle and one 90Ta–10W nozzle had revealed that oxidation of the metal surface in contact with the gaseous products of combustion was a serious problem, the remaining nozzles were coated with silicide oxidation-resistant coatings. This type of coating (consisting of a thin layer of tungsten or tantalum disilicide applied to the metal surface) was considered to represent the best of the currently available oxidation-resistant coatings. The coatings were applied by a pack-cementation process at temperatures below the recrystallization temperature of tungsten.

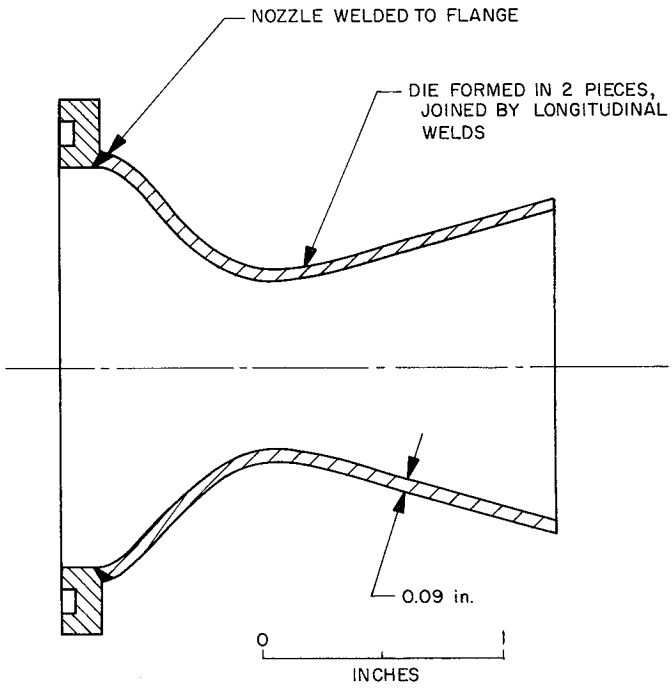


**Fig. 3. Configuration of refractory metal nozzle**

Initial success in testing one of the coated tungsten nozzles indicated that this material showed promise for space engine applications. Accordingly, two complete thrust chambers were fabricated from spun and welded tungsten, as shown in Fig. 4. With the exception of the method of attaching the thrust chamber to the injector,

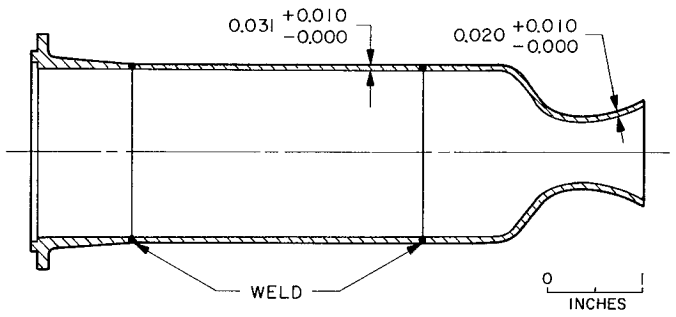


**Fig. 4. Configuration of tungsten thrust chamber**

the design was essentially that of a flight-weight engine. The wall thickness required to contain the chamber pressure in the cylindrical portion was determined from data on the high-temperature tensile strength of wrought tungsten and from an estimate of the equilibrium wall temperature. This thickness was conservatively calculated to be 0.031 in. The thickness of the wall at the nozzle throat was nominally 0.020 in., representing the thinnest section which could be fabricated by conventional techniques. The density of one finished thrust chamber was determined to be 99.5% of theoretical, resulting in a total weight of 1.5 lb. The outer surface of the thrust chamber was machined before welding to provide the required wall thickness, but the inner surface was left as spun. The surfaces of the welds were not machined.

## III. EXPERIMENTAL METHODS

After the materials to be tested had been fabricated into nozzles or thrust chambers, as described in Section II, these components were attached to a research injector for evaluation. Test conditions are summarized in Table 2.

The initial tests in this program were conducted with single-element injectors, supplying concentric, intersecting sheets or sprays of fuel and oxidizer in an effort to ensure uniform circumferential propellant-mass distribution. However, maintaining reasonable injection velocities at low propellant flow rates (resulting from the low thrust level) required extremely small flow passages in the form of thin slots, which could not be accurately controlled. Asymmetric and nonreproducible propellant distribution resulted, producing regions of high local erosion rates in the throats of ablative thrust chambers. Because of the difficulties involved in controlling the flow passages required to produce these thin sheets, two types of injectors incorporating circular liquid jets as the injector element were designed for use in materials tests. All tests reported here were conducted with injectors fabricated to these latter two basic designs.

**Table 2. Test conditions**

| Parameter | Propellants | |
|---|---|---|
| | $N_2O_4/N_2H_4$ | $ClF_3/N_2H_4$ |
| Mixture ratio | 1.0 | 2.2 |
| Chamber pressure, psia | 150 | 150 |
| Theoretical equilibrium exhaust-gas composition at throat, mole % | $H_2O$-40<br>$H_2$-18<br>H-1<br>OH-1<br>$N_2$-40 | $H_2$-10<br>H-4<br>HF-49<br>HCl-13<br>Cl-3<br>$N_2$-21 |
| Theoretical combustion temperature, °F | 4850 | 5771 |
| Theoretical equilibrium characteristic exhaust velocity c*, fps | 5816 | 5874 |

The first of these injector designs, as shown in Fig. 5, is basically one element of an injector which had previously demonstrated high characteristic exhaust velocity $c^*$ with stable combustion at higher thrust levels and higher chamber pressure when used with $ClF_3/N_2H_4$ propellants (Ref. 2). A characteristic of this design is the absence of direct liquid-phase mixing of the propellants, since the fuel jets impinge on the outer splash cup, and the oxidizer jets impinge on the central plug. The circumferential propellant distribution thus produced is fairly uniform, and most of the mixing presumably occurs downstream of the end of the cup as a result of recirculation and secondary flow in the combustion chamber. Two injectors were fabricated to this design, one for testing with $N_2O_4/N_2H_4$ and one for testing with $ClF_3/N_2H_4$, the only difference being the diameter of the orifices.

In the following summary, it is seen that neither version of this "plug-and-cup" injector produced the experimental performance that had been expected from the multi-element experience as reported in Ref. 2; i.e., in the order of 93% of theoretical $c^*$. For example:

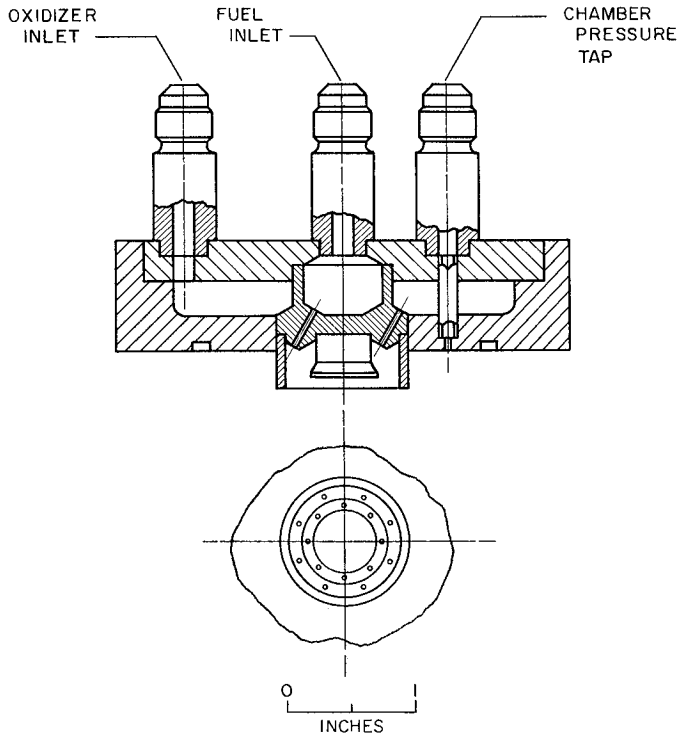


**Fig. 5. Injector used with $ClF_3/N_2H_4$ and $N_2O_4/N_2H_4$**

1. With $ClF_3/N_2H_4$, at a mixture ratio of 2.2, the $c^*$ value was 4500 fps (77% of theoretical shifting equilibrium) at 30-in. $L^*$.

2. With $N_2O_4/N_2H_4$, at a mixture ratio of 1.0, $c^*$ averaged 5000 fps (86% of theoretical shifting equilibrium) at 30-in. $L^*$, and 5050 fps (87% of theoretical) at 42-in. $L^*$.

Although this performance was lower than desired, these injectors were utilized in a number of materials-evaluation tests and served as useful tools for this purpose.

Since early test results indicated that the injector plays an important role in determining local erosion rates, and since the plug-and-cup injector design failed to provide both a high combustion efficiency and an easily understandable mixing–combustion process, a second injector design was developed with the expectation of achieving an adequate performance level, together with sufficient control of the injection process to permit some insight into injector-related erosion mechanisms. Studies at this Laboratory have indicated that, by carefully controlling the hydraulic characteristics of the jets comprising an *unlike impinging doublet* injector element, the characteristics of the spray produced with nonreacting liquids may be related to some characteristics of the combustion in a reacting system. In particular, the relative uniformity of the mass and mixture-ratio distributions across the combustion chamber cross section, as determined with nonreactive liquids, was shown in Ref. 3 to be related to engine performance as characterized by $c^*$ and specific impulse $I_{sp}$. Evaluation of the nonreactive flow properties near the thrust chamber wall should also provide some indication of the flow properties at the wall in the reacting system and thus allow some correlation with erosion data. Accordingly, the injector subsequently developed incorporated the results of these earlier studies. The two versions of this injector, differing only in detail, were designated Mod I and Mod II (Fig. 6).

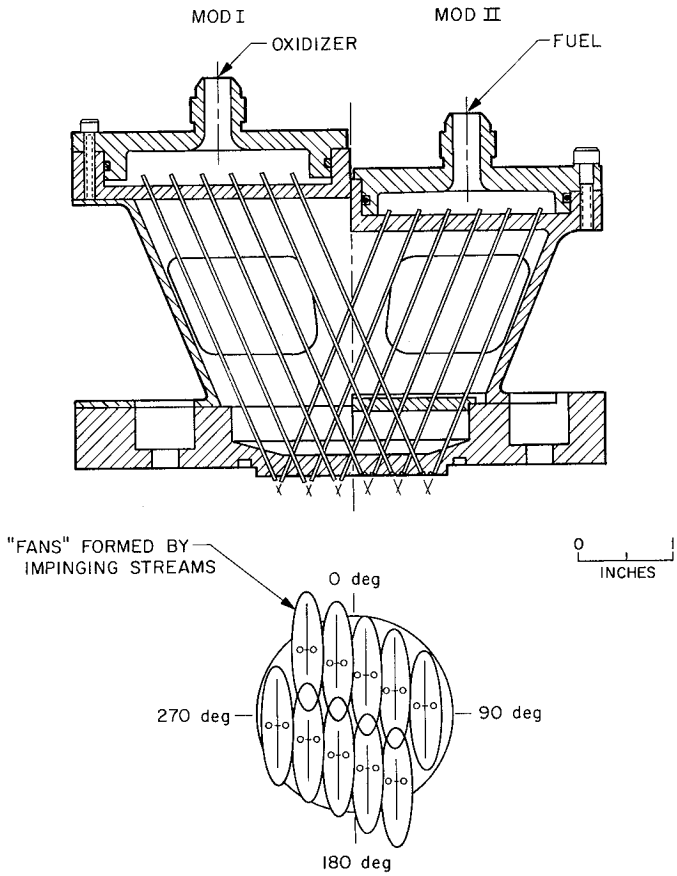


**Fig. 6. Long-tube injectors**

As shown in Fig. 6, the orifices for these injectors consisted of long tubes, designed to provide fully developed turbulent flow of the liquid streams. This flow configuration was shown in Ref. 4 to produce liquid jets which were stable, similar, reproducible, and relatively insensitive to disturbances in the upstream system. The exit ends of the 0.020-in.-I.D. tubes were carefully lapped to remove any burrs which might disturb the flow

leaving the orifice. The arrangement of the 10 pairs of orifices was the same for both injectors and provided a reasonably uniform mass distribution across the cross section of the combustion chamber. Average velocity of the jets was 150 fps for the fuel and 100 fps for the oxidizer.

It should be pointed out that the use of small-diameter orifices of this length with high jet velocities is rather impractical for a flight system, since friction pressure drops become quite large. For example, the total injector pressure drop of the fuel side of the Mod I injector was about 800 psi, of which about 600 psi was estimated to result from friction.

Only two of the detail differences between the Mod I and Mod II injectors concern the hydraulic characteristics of the liquid jets and, hence, the performance of the combusting system. The orifices used in the Mod II injector were 150 diameters long, whereas those in the Mod I injector were 175 diameters long. However, since either orifice was long enough to produce a fully developed turbulent velocity profile, this change would not be expected to influence injector spray characteristics. The second difference involved a change in the free-stream length of the liquid jets before impingement. The orifices on the Mod I injector protruded from the face and were subject to damage during handling between tests. The orifices on the Mod II injector were located flush with the face for protection; however, the impingement point was unchanged, resulting in an increased free-stream jet length before impingement. This free-stream length was 4 jet diameters for the Mod I injector versus 8.5 diameters for the Mod II injector. The effect of this change on spray characteristics was not evaluated, but is assumed to be small.

Using $N_2O_4/N_2H_4$ propellants at a mixture ratio of 1.0 in a combustion chamber having a characteristic length $L^*$ of 42 in., the Mod I injector produced an average $c^*$ of 5620 fps (96.6% of theoretical shifting equilibrium), whereas the Mod II injector produced an average $c^*$ of 5490 fps (94.3% of theoretical). Although the difference in free-stream jet length could be a factor in the lower performance of the Mod II injector, a more likely explanation is that detail differences in machining the injector faces produced differences in orifice alignment for the two injectors, with a resulting variation in mixing and, hence, in mixture-ratio distribution. Alignment of the 0.020-in.-diameter jets was found to be very critical in tests with nonreacting liquids, and a misalignment of less than 0.001 in. in the centerlines of two impinging jets changed the mass and mixture-ratio distributions in the spray to a marked degree. Maximum misalignment of the centerlines of the orifices comprising each doublet element used in these two injectors was of the order of 0.001 in., indicating that alignment differences could affect mixing sufficiently to result in a 2% difference in performance between the two injectors.

This long-tube injector design produced relatively smooth combustion. Chamber pressure oscillations of $\pm$ 4 psi peak-to-peak (at a chamber pressure of 150 psia) were measured for the Mod II injector by means of a high-frequency-response Photocon transducer. A noise-like frequency distribution was observed.

Propellant flow rates were maintained constant during all tests by means of cavitating venturis in the propellant feed lines. Such a venturi ensures that flow rate does not vary with a changing downstream pressure; thus, erosion of the throat of the rocket engine being tested results in a decrease in chamber pressure which may be assumed to be inversely proportional to the change in throat area. During a test, chamber pressure was monitored and used as an indicator of the amount of throat erosion which had taken place. Tests during which severe throat erosion occurred were arbitrarily terminated when chamber pressure had decreased from an initial 150 psia to 120 psia, indicating a 25% increase in throat area. Tests which did not result in throat erosion sufficient to reduce the chamber pressure to 120 psia were terminated after 300 sec. Propellant flow rates were measured with turbine flowmeters, and chamber pressure with a strain-gage transducer. Thrust was not measured.

After testing, the outline of the throat was obtained by tracing on paper the image produced by an optical comparator at a magnification of 10. From this tracing, the final throat area could be determined with a planimeter, and local erosion could be measured by comparing the final outline of the throat with the initial (circular) outline. Chambers and nozzles were then sectioned and examined for internal effects.

# IV. RESULTS

The results of this program may be conveniently divided into two broad but interrelated categories. The first concerns the performance, in a gross sense, of a variety of materials tested under similar conditions in a liquid rocket engine. The erosion rates observed for different materials may be related to the mean-mixed rocket engine environment as characterized by nominal gas composition, average heat-transfer rate, etc., and general conclusions may be reached as to which materials may be suitable for use under a given set of conditions. The second category concerns the local performance of the thrust chamber material as determined by local nonuniformities in the combustion process. These local nonuniformities are originated by the injector and produce effects such as asymmetric throat erosion, usually referred to as "injector streaking." The nonuniform character of the combustion-flow process, although generally acknowledged, is imperfectly understood. It will be seen, however, that injector-related nonuniformities in the combustion process can exert an overriding influence on thrust chamber material performance.

## A. Performance of Materials

Conclusions relating to the performance of the three types of materials tested are summarized below.

### 1. Ablative Materials

*a. Nozzles.* A survey of the performance of some of the reinforced plastics available for use in uncooled thrust chambers was conducted with the plug-and-cup injector (see Fig. 5) and $N_2O_4/N_2H_4$ propellants. One nozzle fabricated from each of the materials of interest was tested. The significant experimental results are summarized in Table 3, and Fig. 7 shows a section of the 90-deg-orientation Refrasil-cloth nozzle after testing, illustrating the construction of the nozzle and the char typical of a 300-sec test.

A wide variety of erosion rates was observed, ranging from negligible ablation in 300-sec tests for the Refrasil nozzles to a throat-area increase of 30% in a 23-sec test for a nozzle fabricated with carbon-cloth reinforcement. Intermediate erosion rates were observed for nozzles reinforced with graphite cloth, asbestos cloth, and zirconium oxide fiber.

Although low erosion rates were observed with Refrasil reinforcement in all the forms tested, it appeared that some orientations may be more desirable than others. For example, nozzles fabricated of randomly oriented ½-in. squares of Refrasil cloth tended to present a rough surface to the gas flow, whereas a smooth, evenly ablating surface is desirable for accurate control of thrust-vector orientation. Nozzles fabricated from unoriented Refrasil fibers and macerated Refrasil also exhibited a more uneven surface than did nozzles made from cloth laminates. Although these effects would be less objectionable in large-diameter nozzles, they are undesirable for low-thrust engines of the types of interest, since small surface irregularities may produce appre-

**Table 3. Results of tests of ablative nozzles**

| Material[a] | Test[b] duration, sec | Area change, % | Char depth at throat, in. | Average erosion rate, mils/sec |
|---|---|---|---|---|
| Refrasil cloth–phenolic, laminated at 90 deg | 300 | −4 | 0.60 | — |
| Refrasil cloth–phenolic, laminated at 60 deg | 301 | −14 | 0.55 | — |
| Refrasil cloth-phenolic plus volcanic ash, laminated at 60 deg | 303 | −4 | 0.42 | — |
| Chopped Refrasil (½-in. squares)–phenolic | 301 | −12 | 0.66 | — |
| Chopped Refrasil (½-in. squares)–phenolic plus volcanic ash | 301 | −7 | 0.57 | — |
| Macerated Refrasil fiber–phenolic | 251 | +7 | 0.41 | 0.05 |
| ¼-in. Refrasil fiber–phenolic | 300 | −13 | 0.55 | — |
| Zirconium oxide fiber–phenolic | 114 | +24 | 0.34 | 0.39 |
| Asbestos cloth–phenolic, laminated at 60 deg | 30 | +20 | 0.09 | 1.3 |
| Graphite cloth–phenolic, laminated at 90 deg | 82 | +21 | 0.60 | 0.49 |
| Graphite cloth–phenolic, laminated at 60 deg | 117 | +23 | 0.70 | 0.41 |
| Chopped graphite cloth (½-in. squares)–phenolic | 42 | +22 | 0.39 | 1.0 |
| Carbon cloth–phenolic, laminated at 90 deg | 23 | +30 | 0.14 | 2.4 |

[a]Supplied by H. I. Thompson Fiber Glass Co., Los Angeles, California.
[b]$N_2O_4/N_2H_4$ propellants; plug-and-cup injector; M.R. = 1.0; $P_c$ = 150 psia; $L^*$ = 42 in.; $c^*$ = 5050 fps.

ciable components of thrust normal to the intended thrust direction. In small sizes, such as those considered here, the cloth laminates appear to give the best results.

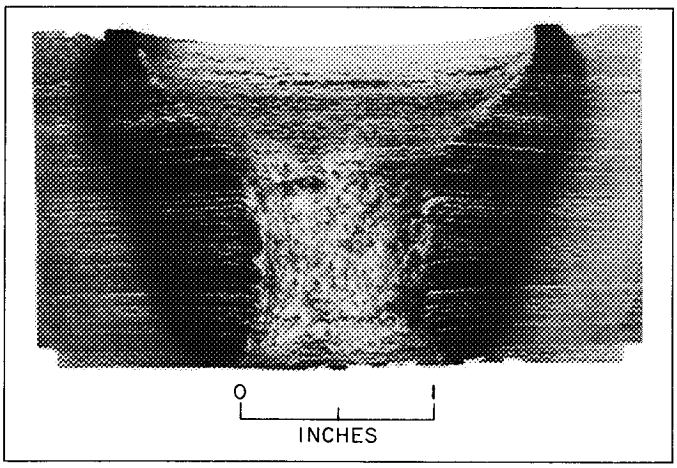


**Fig. 7. Sectioned view of ablative nozzle after testing**

The char depths listed in Table 3 are those of the visible char: i.e., the depth to which a char layer may be distinguished by discoloration of the plastic or, in the case of the carbon and graphite cloth laminates, by porosity of the charred resin. The addition of volcanic ash to the phenolic resin in Refrasil nozzles reduced the char depth slightly, but resulted in a small increase in ablation rate. Changing the orientation of the cloth laminate from 90 to 60 deg resulted in a small reduction in char depth as measured normal to the nozzle axis. This result was to be expected, since the thermal conductivity is higher along the fibers than across the fiber–resin boundaries.

The high erosion rate of the asbestos nozzle is consistent with results of other tests of this material in various types of high-temperature, high-heat-flux environments. However, the relatively high erosion rate exhibited by the nozzle reinforced with zirconium oxide fiber presents an anomaly, since the relatively high melting point of this material (about 4900°F, as compared with 3000–3500°F for silica) would be expected to result in a superior reinforcement material. The vendor who supplied the nozzle has suggested that the fabrication technique used may have been inadequate, and that further attempts could conceivably produce a more erosion-resistant molding. The fabrication method resulted in reduction of the fibers to short lengths, about one fiber diameter long. The molding was thus comparable to the macerated Refrasil nozzle (fabricated of short lengths of Refrasil fiber), except that the zirconium oxide fibers were several times the diameter of the Refrasil fibers. The Refrasil nozzle exhibited a much lower erosion rate than the zirconium oxide unit, indicating that the difference in fiber size may be significant. To resolve this discrepancy, however, additional testing is indicated.

Evaluation of the relative erosion resistance of this particular group of materials was complicated by indications that the throat of the Refrasil nozzles shrank during initial heating. This effect was evidenced by an *increase* in chamber pressure during the early portions of the tests which was generally of such magnitude that subsequent erosion did not produce a net throat-area increase in 300 sec of operation. Shrinkage may also have occurred during tests of materials other than Refrasil; however, no increase in chamber pressure was observed, and any shrinkage tending to produce a decrease in throat diameter could easily have been masked by simultaneous erosion. In the nozzle fabricated of Refrasil-cloth oriented at a 60-deg trailing angle to the gas flow, throat shrinkage was particularly severe because delamination produced an additional decrease in throat area. In this case, chamber pressure increased approximately 20 psi during the first 2 min of testing, indicating an area change of 12% and a decrease in throat diameter of about 0.045 in. However, chamber pressure increases of 10 psi were the more usual result in tests of Refrasil nozzles. Some caution is indicated, then, in comparing the relative erosion resistance of various reinforced plastics by examining only the initial and final throat areas, and more information on the rates and mechanisms of shrinkage (as related to the manufacturing technique, in particular) would be desirable. The Refrasil-reinforced materials are, however, clearly the most "erosion"-resistant of the materials tested in the particular environment reported here.

In addition to the effects of throat shrinkage on erosion rate, some consideration must also be given to the particular environment produced by the rocket engine used in these tests. As a first approximation, an average combustion chamber gas temperature $T_c$ may be calculated by assuming

$$T_c = \left(\frac{c^*}{c^*_{theo}}\right)^2 T_{c_{theo}}$$

Using the theoretical $T_c$ of 4850°F for $N_2O_4/N_2H_4$ at a mixture ratio of 1.0 and a $c^*$ for the plug-and-cup injector of 87% of theoretical, an average gas temperature

of 3560°F is computed. A recovery factor of 0.9 (assuming a turbulent boundary layer) would then result in an adiabatic wall temperature of 3500°F at the nozzle throat; this is only slightly above the temperature at which Refrasil (which is more than 99% $SiO_2$) begins to flow. Since the adiabatic wall temperature represents the *maximum* temperature which the wall could attain (i.e., if the wall were a perfect insulator), little melting of the silica would be expected and, indeed, charring ablation was experienced. However, in the environment produced by a high-performance injector, the erosion rates of all the materials tested would undoubtedly be higher, simply because heat-transfer rates and, hence, wall temperatures would be higher.

Since tests of these same reinforced plastics as solid rocket nozzle inserts have demonstrated somewhat different relative erosion resistance from that reported here, it is instructive to compare the environments produced within the solid and the liquid motors, in order to gain some insight into the mechanisms which control nozzle erosion. The solid rocket motor environment may be characterized as one producing higher throat heat fluxes and shear forces than those occurring in the types of liquid rocket engines considered here. These differences stem primarily from the higher chamber pressures (and resultant higher mass flow rates) and higher equilibrium gas temperatures used in solid rockets. Thus, the thermal input to the wall and, as a result, the "equilibrium" wall temperature would be expected to be higher in the solid rocket. The equilibrium gas composition within the aluminized solid propellant rocket motor is generally reducing in nature, since the available oxygen combines with the aluminum to form $Al_2O_3$. The chemical environment within the $N_2O_4/N_2H_4$ liquid rocket, on the other hand, is oxidizing in nature, even at nominal mixture ratios below stoichiometric, since the equilibrium products of combustion contain large quantities of water vapor.

These differences in thermal and chemical environments, when examined in conjunction with the properties of the nozzle material, may reasonably be expected to account for the differing relative erosion resistance exhibited by the various reinforced plastics when tested in solid and in liquid rocket engines. For example, carbon and graphite-cloth nozzles eroded rapidly in the $N_2O_4/N_2H_4$ liquid rocket engine, but are widely used in aluminized solid propellant rocket nozzles, where they display superior erosion resistance. Since carbon reacts readily with water vapor at high temperatures, the "erosion" observed is most probably the result of this chemical reaction between the nozzle wall reinforcement material and $H_2O$ in the products of combustion. Refrasil-reinforced laminates, which exhibited negligible erosion in the $N_2O_4/N_2H_4$ nozzle tests, erode rapidly when used as throat inserts in solid rocket engines where the thermal input is high enough to produce melting (i.e., ablation). Although a carbonaceous char is produced during heating, the melting silica probably tends to protect the char from the combustion products, and chemical reactions in the $N_2O_4/N_2H_4$ system apparently proceed slowly, if at all.

***b. Thrust chambers.*** In addition to tests of ablative nozzles, complete Refrasil–phenolic ablative thrust chambers of the type shown in Fig. 1(a) were tested with both the Mod I and the Mod II version of the long-tube injector, as well as with the plug-and-cup injector. In the case of the plug-and-cup injector, tests were conducted with $ClF_3/N_2H_4$ propellants, and also with $N_2O_4/N_2H_4$. Results of these tests are summarized in Table 4.

The most striking result of this group of tests is the marked difference between the low erosion rate produced by the plug-and-cup injector and the erosion rates produced by the long-tube injectors, even though the gross system characteristics (i.e., propellant combination, mixture ratio, and chamber pressure) were identical. Using $N_2O_4/N_2H_4$ propellants, an ablative thrust chamber tested with the plug-and-cup injector experienced no net throat erosion in 235 sec, at which time the engine failed at the joint between the nozzle and the combustion chamber. This result is comparable to those reported for the nozzle tests, where no net erosion was observed with Refrasil–phenolic laminates when tested with the same injector. Ablative thrust chambers tested with the two long-tube injectors, however, experienced throat-area changes of about 30% in approximately 30 sec of testing. Local erosion rates as high as 5 mils/sec were observed in these tests, with an "average" erosion rate (based on distributing the asymmetric area change evenly around the circumference of the throat) of 2.0 mils/sec for the Mod I injector and 1.8 mils/sec for the Mod II injector. Ablation characteristically produced melting of the silica at the throat, the viscous liquid collecting in the exit portion of the nozzle, where it solidified after a test. Using the same approximations as those mentioned previously in calculating an adiabatic wall temperature associated with the plug-and-cup injector, nozzle-throat adiabatic wall temperatures of 4500°F for the Mod I injector and 4250°F for the Mod II injector may be computed. Note that both of these temperatures are well above the temperature at which silica begins to flow (about 3200 °F), indicating that some melting with attendant dimensional

**Table 4. Results of tests of ablative thrust chambers[a]**

| Propellants | Mixture ratio | Injector | L*, in. | c*, fps | Initial chamber pressure, psia | Test duration, sec | Area change, % | Char depth at throat, in. | Average erosion rate, mils/sec |
|---|---|---|---|---|---|---|---|---|---|
| $N_2O_4/N_2H_4$ | 1.0 | Long-tube Mod I | 42 | 5620[b] | 153 | 29 | +30 | 0.18–0.23 | 2.0 |
| $N_2O_4/N_2H_4$ | 1.0 | Long-tube Mod II | 42 | 5490[b] | 149 | 30 | +28 | 0.18–0.28 | 1.8 |
| $N_2O_4/N_2H_4$ | 1.0 | Plug and cup | 30 | 5000[b] | 148 | 235 | −6 | 0.55 | — |
| $ClF_3/N_2H_4$ | 2.2 | Plug and cup | 30 | 4300[c] | 113 | 267 | +30 | 0.60 | 0.21 |
| $ClF_3/N_2H_4$ | 2.2 | Plug and cup | 30 | 4500[c] | 148 | 165 | +15 | 0.55 | 0.17 |

[a]Manufactured by Douglas Aircraft Co., Santa Monica, California.
[b]Average value recorded in tests with nonablating nozzles.
[c]Value for this test using original ablative throat area.

change would be expected. It must be emphasized that these approximate calculations neglect many important considerations, such as the effect of injection of gases into the boundary layer by the charring resin, as well as effects of injector nonuniformities. They do serve, however, to illustrate the importance of injector performance on material behavior. The relationship between the asymmetric erosion pattern produced by the Mod II injector and some of the characteristics of this injector is discussed in subsection IV-B, below.

Tests of two thrust chambers with the plug-and-cup injector and $ClF_3/N_2H_4$ propellants resulted in higher throat-erosion rates than those obtained when the same injector design was used with $N_2O_4/N_2H_4$ propellants. The thrust chamber which was tested for 267 sec again failed at the chamber–nozzle joint. An approximation of the heat flux at the nozzle throat (using the method of Ref. 5) indicates that, in these tests, the heat fluxes for $N_2O_4/N_2H_4$ and $ClF_3/N_2H_4$ were about the same. The very low performance exhibited during the $ClF_3/N_2H_4$ tests counterbalanced the higher heat fluxes generally associated with this system and, as a result, cold-wall throat heat fluxes of about 5 Btu/in.$^2$-sec are predicted for either propellant combination. This would indicate that the higher throat-erosion rates observed during tests with $ClF_3/N_2H_4$ may well have resulted from chemical attack of the silica fibers (which comprise the Refrasil reinforcement) by hydrogen fluoride in the exhaust products.

As is evident from the results of the long-duration tests of the ablative thrust chambers, the design of the joint between the combustion chamber and the nozzle was inadequate and contributed to several thrust chamber failures. Prolonged exposure to the hot combustion products caused the simple butt joint between the two Refrasil moldings to expand and erode slightly, thus allowing the hot gases to reach the insulating layer and, eventually, the outer wrap, producing a pressure-vessel type of failure as the outer wrap was heated and weakened.

Shrinkage of the nozzle throat during initial heating was less pronounced with the ablative thrust chambers than with the Refrasil nozzles discussed above, indicating that fabricating techniques are available which can minimize this effect. The amount of shrinkage is presumably related to the cure and postcure cycle employed during fabrication.

Combustion chambers constructed with fibers in either the 45-deg trailing orientation or the 90-deg orientation (i.e., perpendicular to the chamber axis) exhibited negligible erosion during all tests of the ablative thrust chambers. In fact, as a result of low rates of heat transfer to the combustion chamber wall (a consequence of the high contraction area ratio—the average Mach number in the combustion chamber, for example, was only 0.1), ablation involving a dimensional change was confined to the region of the nozzle throat during all tests of Refrasil–

reinforced materials. In an ablative throat, however, a dimensional change appears probable at high performance (i.e., high $c^*$) for both the $ClF_3/N_2H_4$ and $N_2O_4/N_2H_4$ propellant combinations at this chamber pressure level unless the injector can be controlled to ensure low rates of heat transfer to the wall. Two other methods of minimizing the change in throat area would be:

1. Lowering of the operating chamber pressure (and, hence, the heat flux) to a level which would permit the throat material to act as a charring ablator.
2. Use of an insert of a nonablating material at the throat.

A throat insert of graphite, for example, should be most suitable for the $ClF_3/N_2H_4$ propellant combination. Reference 6 indicates that carbon is relatively inert in HF atmospheres at probable rocket engine wall temperatures.

In summary, these results indicate that Refrasil-cloth–phenolic-resin laminates are the most erosion-resistant of the materials tested in the $N_2O_4/N_2H_4$ rocket engine environment. However, heat-transfer rates in an engine producing high combustion efficiency (i.e., high $c^*$) at a chamber pressure of 150 psia may be high enough to raise the wall temperature above the melting point and produce rapid erosion of Refrasil nozzle throats.

## 2. Graphites

Two graphite-backed pyrolytic graphite nozzle assemblies and two freestanding pyrolytic graphite thrust chambers were tested, together with several nozzles fabricated completely of ordinary graphite. Results of all these tests are summarized in Table 5.

***a. Pyrolytic graphic nozzles.*** As shown in Table 5, one of the graphite-backed pyrolytic graphite nozzle assemblies was tested with each of the two basic injector designs. The nozzle tested with the plug-and-cup injector sustained a 300-sec test with a throat-area increase of 5% for an average erosion depth of 0.009 in. (i.e., 0.03 mil/sec). Sectioning of the nozzle after testing revealed some delamination, but no radial cracks were evident. The throat erosion which did occur was probably a result of oxidation by water vapor in the exhaust products, as in the case of the plastic nozzles reinforced with carbon and graphite cloth.

The nozzle tested with the long-tube injector (Mod I, in this case) cracked during testing, as illustrated in Fig. 8. Hot gas, escaping through the crack, eroded a path through the substrate, resulting in erosion of the pyrolytic shell, as shown in the photograph.

***b. Pyrolytic graphite thrust chambers.*** Both freestanding pyrolytic graphite thrust chambers were tested with the Mod II long-tube injector for short durations at a

**Table 5. Results of tests of graphite thrust chambers and nozzles**

| Material | Configuration | Injector | Test[d] duration, sec | Area change, % | Average erosion rate, mils/sec |
|---|---|---|---|---|---|
| Pyrolytic[a] (backed) | Nozzle | Mod I | 149 | Cracked | Cracked |
| Pyrolytic[a] (backed) | Nozzle | Plug and cup | 300 | +5 | 0.03 |
| Pyrolytic[b] (free standing) | Thrust chamber | Mod II | 30 | −0 | 0.5 max |
| | | | 30 | −0 | 0.5 max |
| | | | 21 | Failed | Failed |
| Pyrolytic[b] (free standing) | Thrust chamber | Mod II | 44 | Failed | Failed |
| ATJ[c] | Nozzle | Mod I | 71 | +22 | 0.60 |
| ZT[c] | Nozzle | Mod I | 96 | +33 | 0.65 |
| ATJ | Nozzle | Plug and cup | 160 | +22 | 0.26 |
| ZT | Nozzle | Plug and cup | 157 | +28 | 0.33 |

[a]Manufactured by Raytheon Co., Waltham, Massachusetts.
[b]Manufactured by High Temperature Materials Inc., Boston, Massachusetts.
[c]Manufactured by National Carbon Co., New York.
[d]$N_2O_4/N_2H_4$ propellants; M.R. = 1.0; $P_c$ = 150 psia (140 psia in tests of freestanding thrust chambers); $L^*$ = 42 in.; $c^*$: Mod I = 5620 fps, Mod II = 5490 fps, Plug and cup = 5050 fps.

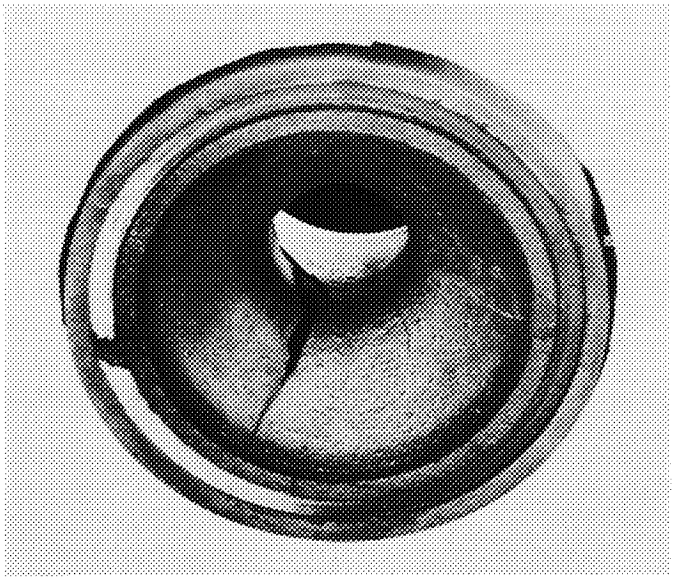

**Fig. 8. Pyrolytic graphite nozzle after testing**

chamber pressure of 140 psia. One chamber was tested three times; the first two tests were each of 30 sec duration, with local erosion occurring in one area of the throat to a depth of 0.015 in. (i.e., 0.5 mil/sec) during each test and comparable local erosion depths in some areas near the injector. Between the two tests, this thrust chamber was rotated in relation to the injector, in order to distribute the erosion around the circumference of the chamber wall. The thrust chamber then failed during a third test, after 21 sec of operation. The chamber was not rotated between the second and third tests, so that erosion at the worst locations was cumulative over 51 sec of firing. Figure 9 shows this thrust chamber during a test (the image at the lower right resulted from a mirror placed behind the engine). The second freestanding thrust chamber failed during the initial test after 45 sec of operation.

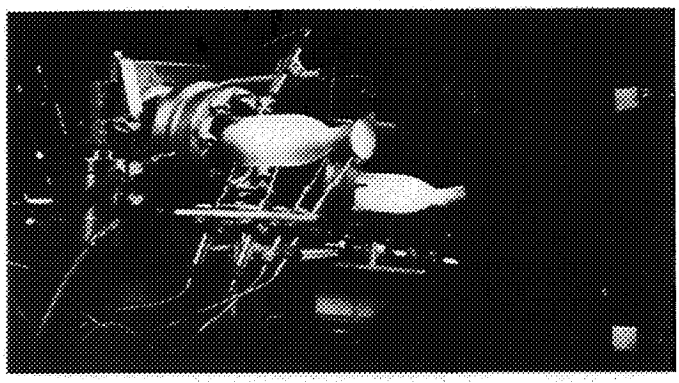

**Fig. 9. Pyrolytic graphite thrust chamber during test**

Failure of both thrust chambers was characterized by complete shattering of the combustion chamber, although the nozzle exit cone was recovered intact in both cases. High-speed motion pictures taken during the tests indicated that the failures originated in the combustion chamber, rather than in the throat, which explains the undamaged condition of the exit cone. However, the movies failed to pinpoint the origin of the failures, and, since the thrust chambers were so completely shattered as to defy reconstruction, a failure analysis is necessarily somewhat speculative. Failure in both cases probably resulted from the interaction of two effects: (1) erosion of the combustion chamber wall to a point where the hoop stress approached (but probably did not exceed) the ultimate tensile strength, and (2) temperature gradients and resulting thermal stresses in the chamber wall. The magnitude of local erosion near the injector was comparable with that of erosion in the nozzle throat, indicating that, in some areas, the wall was thinned from an initial thickness of approximately 0.050 in. to a thickness of the order of 0.025 in. at the time of failure. Thermal stresses (which cannot be relieved by yielding in the case of a brittle material such as pyrolytic graphite) plus any delamination which might have been present could have produced failures in these thin sections of the combustion chambers.

These tests indicate that, given an adequate development cycle during which the thermal stresses associated with a particular design can be minimized, pyrolytic graphite would probably be suitable as a thrust chamber material. Adequate control of the injector would be desirable, however, to minimize oxidizing regions and wall-temperature variations. Other pyrolytic materials now being developed, such as alloys of boron and graphite, may prove more desirable than pyrolytic graphite for thrust chamber applications.

*c. Normal graphite nozzles.* Tests of normal high-density graphite nozzles demonstrated erosion rates up to an order of magnitude higher than the erosion rates observed in comparable tests of pyrolytic graphite components. The erosion rate of ZT graphite was comparable to that of ATJ graphite, but the more homogeneous composition of the ZT grade resulted in a considerably smoother eroded surface. Although the static oxidation rate of pyrolytic graphite is comparable to that of normal graphites at high temperatures (Ref. 7), the oxidation of pitch–coke graphites such as ZT and ATJ proceeds preferentially in the pitch or binder phase (Ref. 8), allowing grains to be physically removed by aerodynamic shear forces. The "erosion" rate of the normal

graphites in a fast-moving oxidizing atmosphere would thus be expected to be higher than that of pyrolytic graphite, as was observed to be the case. High-density graphites, such as the ATJ and ZT grades tested here, are commonly used as throat-insert materials in aluminized solid propellant rocket motors, demonstrating superior erosion resistance under nonoxidizing conditions.

### 3. Refractory Metals

Four refractory metal nozzles and two refractory metal thrust chambers were tested, all with the two long-tube injectors. Results of these tests are summarized in Table 6.

*a. Nozzles.* Tests of uncoated nozzles of both tungsten and 90Ta–10W alloy resulted in similar failures when, in each case, a hole was eroded through the nozzle wall just upstream of the throat. Both burnouts occurred at the same angular location relative to the injector pattern, suggesting that the failures were related to asymmetries in the injection–combustion process. The failed 90Ta–10W nozzle is shown in Fig. 10. Deposits inside this nozzle, downstream of the eroded area, were analyzed as $Ta_2O_5$, indicating that the burnout was the result of oxidation of the nozzle wall by the combustion products. No such deposits remained on the tungsten nozzle, since the oxides of tungsten are volatile at the temperatures encountered in these tests. A thermocouple spot-welded to the outer wall of the tungsten thrust chamber at the throat recorded a temperature of 3100°F during the test; however, this should not be interpreted as the actual wall temperature, since the reading is uncorrected for losses. The true wall temperature could be as much as several hundred degrees higher.

On the basis of these tests of uncoated nozzles, one nozzle of each material was coated with a silicide diffusion coating to improve oxidation resistance. When tested under the same conditions as those used for the uncoated nozzles, the 90Ta–10W nozzle again failed locally, although the firing duration to failure was 182 sec as against 45 sec for the uncoated nozzle. The mechanism of failure again appeared to be oxidation of the base material. The coated tungsten nozzle was tested for 300 sec with no erosion and only minor coating damage, consisting of a pinhole failure on the outer wall and small cracks on the inner wall of the nozzle entrance. This nozzle was again tested for 300 sec with no erosion

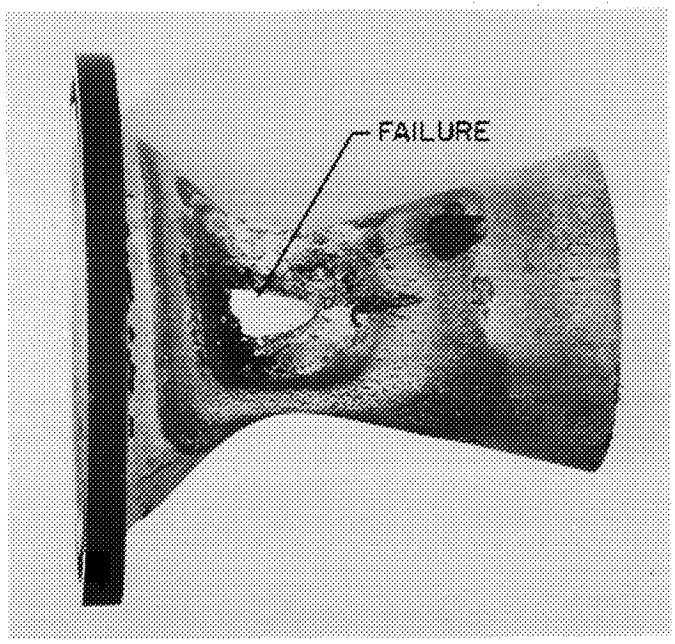


**Fig. 10. Failed 90Ta–10W nozzle after testing**

**Table 6. Results of tests of refractory metal thrust chambers and nozzles**

| Material[a] | Configuration | Injector | Test[b] duration, sec | Comments |
|---|---|---|---|---|
| Tungsten (uncoated) | Nozzle | Mod I | 79 | Burnthrough in throat |
| Tungsten (coated) | Nozzle | Mod I | 300 | No erosion in 2 tests, 300 sec each |
| 90Ta–10W (uncoated) | Nozzle | Mod I | 45 | Burnthrough in throat |
| 90Ta–10W (coated) | Nozzle | Mod I | 182 | Burnthrough in throat |
| Tungsten (coated) | Thrust chamber | Mod II | 2 | Failure in combustion chamber |
| Tungsten (coated) | Thrust chamber | Mod II | <1 | Failure in throat |

[a]Nozzles and thrust chambers fabricated by Super-Temp Corporation, Santa Fe Springs, California. Coatings applied by Chromizing Corporation, Hawthorne, California and Thermomet Diffusion Alloys, Los Angeles, California.

[b]$N_2O_4/N_2H_4$ propellants; M.R. = 1.0; $P_c$ = 150 psia; $L^*$ = 42 in.; $c^*$: Mod I = 5620 fps, Mod II = 5490 fps.

and no change in appearance except for increased oxidation of the exposed tungsten at the pinhole in the coating. The cracks in the coating on the inner surface were unchanged in appearance. Sectioning and dye-penetrant inspection following this second test revealed several hairline cracks in the welds; however, it is not known whether these cracks were present prior to this test and, therefore, whether the cracks resulted from the first or the second firing.

***b. Thrust chambers.*** Success of the coated tungsten nozzle prompted the procurement of two thin-wall spun and welded tungsten thrust chambers. Primary goals of this effort were to investigate the problems associated with the thin-wall fabrication and to continue evaluation of the silicide type of oxidation-resistant coating. Tests of both thrust chambers resulted in rapid failures of the "thermal-shock" variety.

The failure shown in Fig. 11 occurred after about 2 sec of testing. This chamber had been inspected by dye-penetrant techniques and found to be free of cracks. Sections of the failed thrust chamber examined under magnification indicated no flaws, although the finish on the inner surface was somewhat rough. The thrust chamber had been coated on all surfaces with a silicide oxidation-resistant coating; however, there was no evidence that the coating (or the application process involved) contributed to the failure.

The failure of the second thin-wall thrust chamber, shown in Fig. 12, occurred after less than 1 sec of testing. Dye-penetrant inspection of this thrust chamber before testing had revealed porosity of the wall in the convergent section of the nozzle where the failure occurred, the porosity being observed both before and after coating with a disilicide type of oxidation-resistant coating. A cross section of the throat in the region of failure is shown in Fig. 13. The extremely rough inner surface is a result of the fabrication technique, which involved spinning the material onto a male mandrel and machining the outer surface to obtain the proper wall thickness, leaving the inner surface as spun. The cracks shown in Fig. 13 were visible in the untested nozzle as fissures extending axially along the inner surface of the throat section. An attempt was made to polish out these fissures before application of the coating, but the cracks were much too deep to be completely removed. Failure of the

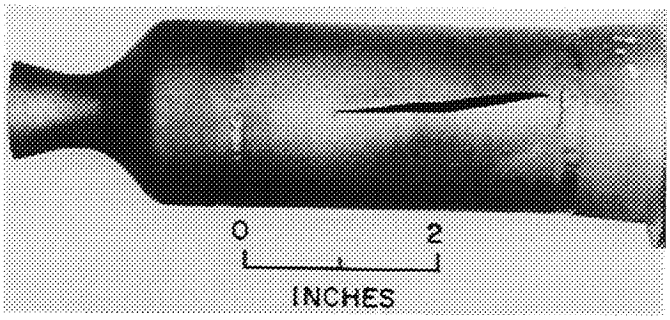


**Fig. 11. Tungsten thrust chamber after testing, showing failure in combustion chamber**

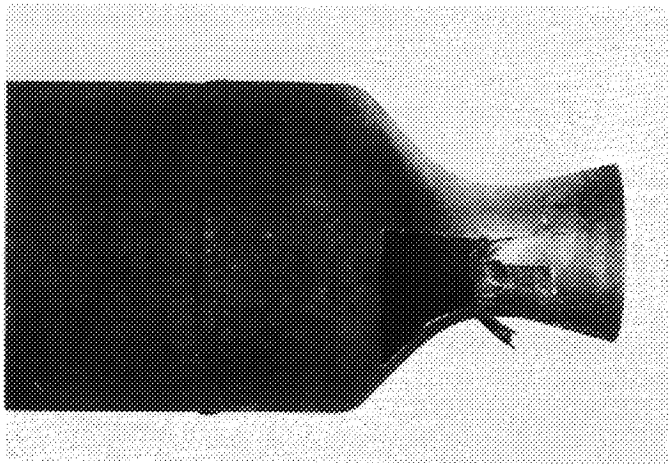

**Fig. 12. Tungsten thrust chamber after testing, showing failure at throat**

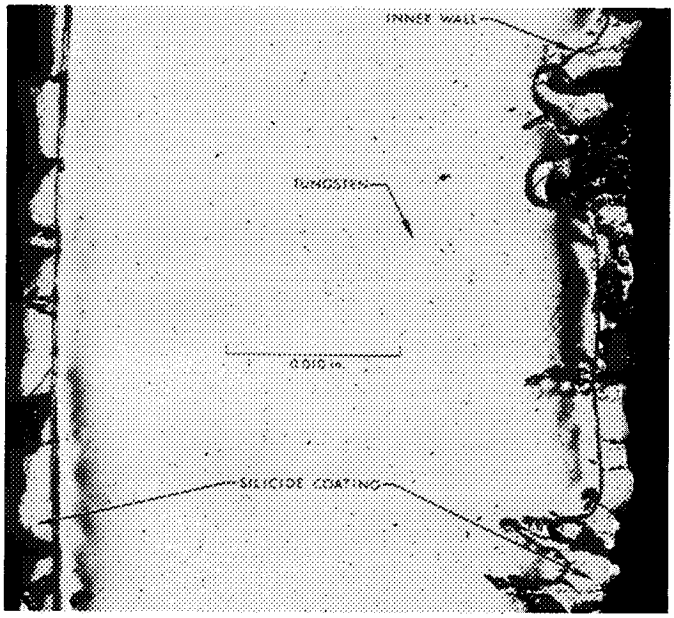


**Fig. 13. Section of wall at throat of tungsten thrust chamber**

thrust chamber originated as a series of axial cracks in the converging section of the nozzle, with transverse cracks resulting in sections of the wall being blown out. The failure occurred very early in the test, before full chamber pressure was reached, and it may be assumed that the temperature of the wall was only slightly above ambient and well below the brittle–ductile transition point. The failure, therefore, may be logically attributed to the fact that stress concentration resulting from the deep cracks on the inner surface of the nozzle produced a brittle failure of the chamber wall. The evidence of porosity found during dye-penetrant inspection before firing indicates that some of the cracks were more severe than those shown in the cross section and actually penetrated completely through the nozzle wall.

Results of these tests with thin-wall thrust chambers indicate that the problems associated with tungsten are similar to some of the problems associated with pyrolytic graphite: i.e., a development cycle is required to overcome problems induced by the brittle nature of the material. The nature of the failures observed indicates that surface finish is all-important with tungsten. Development of a suitable high-temperature oxidation-resistant coating for tantalum alloys would be most desirable, since these alloys are much easier to fabricate than tungsten and, because they are ductile, would be expected to be less susceptible to thermal-stress failures during operation.

## B. Injector-Related Effects

As mentioned above, initial test results showed a marked dependence of the local erosion rates in an ablative throat on injector characteristics, and prompted design of the long-tube injectors, with the aim of providing a controlled, reproducible injection method which could be used to investigate injector-related erosion effects. Approximations to the local thermal and chemical environments produced by the Mod II injector near the thrust chamber wall were determined by two experimental techniques:

1. The characteristics of the spray produced by the 10 doublet injector elements were investigated by flowing nonreacting liquids in place of propellants and sampling the spray produced.

2. Local heat-transfer rates to the chamber wall in the operating rocket engine were measured, using thermocouples embedded in the wall and a transient-heat-conduction analysis.

### 1. Nonreactive Spray Properties

Nonreacting liquids with physical properties similar to those of the propellants were substituted during tests in which the spray produced by the Mod II injector was sampled. The hydrazine fuel (specific gravity = 1.01) was simulated with water (S.G. = 1.00), and the $N_2O_4$ oxidizer (S.G. = 1.45) with a mixture of carbon tetrachloride and kerosene (S.G. of mixture = 1.45). These fluids were injected at the same flow rates as those used for the propellants in the reacting system. The sampling device consisted of a row of sharp-edged ¼-in.-diameter tubes oriented in a position perpendicular to the injector face, with the centerline of the center tube coincident with the centerline of the injector face. A shutter prevented the spray from entering the collector while flow rates were being established. When the shutter was opened, each ¼-in. tube collected a portion of the spray for a known time period. The fluid collected was passed to a graduated test tube where the water and carbon-tetrachloride–kerosene mix, being immiscible, separated. The volume of each liquid was recorded, and the local mass flow rate and mixture ratio were calculated. By rotating the injector in relation to the row of tubes between flow tests, the mass and mixture-ratio distributions across the entire injector pattern were obtained.

Figure 14 shows the mass distribution for the Mod II injector as determined with nonreactive liquids at a distance of 2.13 in. from the injector face. The point marked "100%" represents the maximum local flow rate measured, and the contours denote local flow rate as a percentage of this maximum. No chamber wall was used during these tests, and the spray was allowed to spread beyond the boundary of the operating combustion chamber. The effect of a combustion chamber wall would have been to intercept portions of the spray at a radius of 1 in. and increase the local mass flow rate near the wall.

Figure 15 shows the "nonreactive" mixture-ratio distribution obtained at the same distance (2.13 in. from the injector face), with contours denoting lines of constant mixture ratio. Of particular significance are a region of high mixture ratio near the chamber wall between 350 and 140 deg and an area of low mixture ratio symmetrically opposite. A chamber wall at a radius of 1 in. would have altered this distribution in detail only, since the lines of constant mixture ratio are nearly radial near the boundary. Although this distribution was obtained at a station approximately 40% of the chamber length downstream of the injector face, a similar (but more diffuse) distribution was obtained near the nozzle inlet.

The character of the mixture-ratio distribution would be expected to be similar in the throat also, since the impinging doublet elements produce a minimum of secondary flows, and mixture-ratio gradients tend to propagate undisturbed in the axial direction.

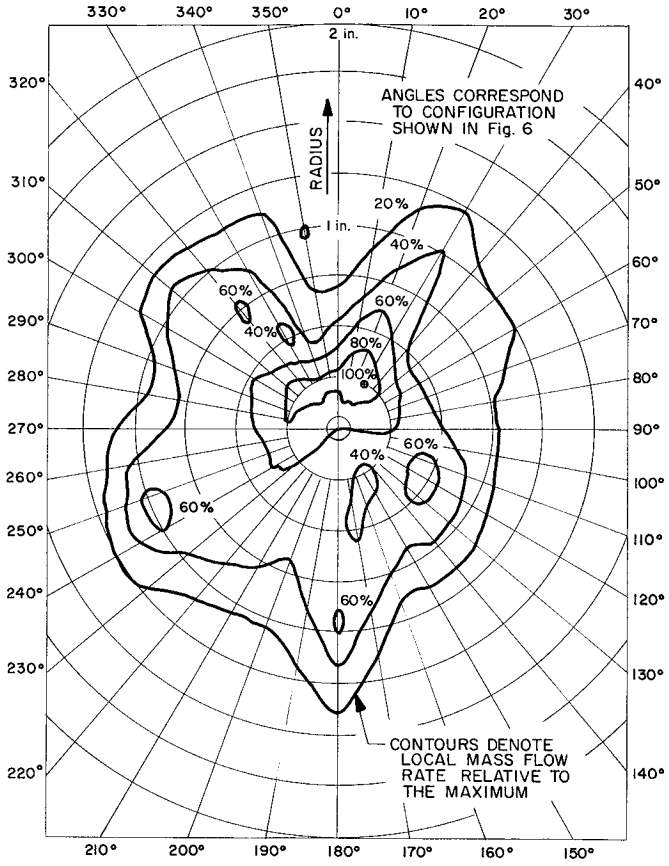


**Fig. 14. Mass distribution for Mod II injector**

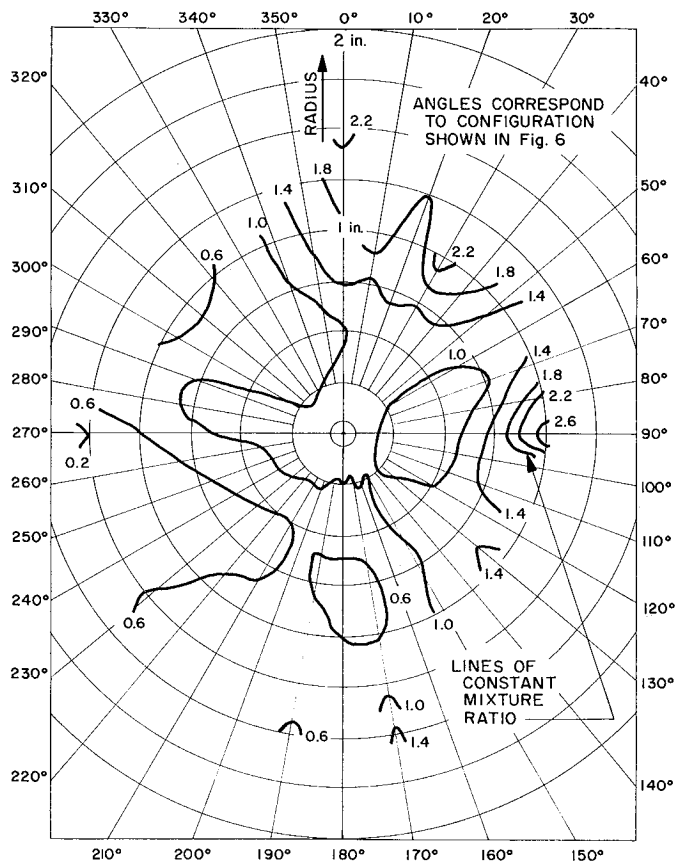


**Fig. 15. Mixture-ratio distribution for Mod II injector**

These mass and mixture-ratio distributions indicate that most of the injected propellant is confined to the region near the axis of the combustion chamber, and that the mixture ratio in this central core is near the nominal (input) mixture ratio of 1.0. The mixture ratio near the wall varies considerably from the nominal, with about one-half of the circumference oxidizer-rich, and one-half fuel-rich. This variation in mixture ratio near the wall is a consequence of the nonuniformity of mixture ratio within the spray "fans" formed by the individual doublet elements. Nonreactive tests of single doublet elements (Ref. 9) have shown that the mixture ratio in the spray is highest on the side of the fan opposite the oxidizer orifice and vice versa. Thus, the streams penetrate one another and the mixture ratio within the spray is reversed from that indicated by the geometry of the incoming jets. It may be seen, then, that those portions of the spray fans which interact with one another (i.e., in the center of the injector pattern as in Fig. 6) combine to produce the nominal mixture ratio, while the portions of the spray near the wall retain the nonuniform character of the appropriate portion of the original fan. (Thus, the chemical composition of the flow near the wall could be controlled by orienting the elements so that either the fuel-rich or the oxidizer-rich side of the spray fan is closest to the chamber boundary.) The relatively high $c^*$ produced by this injector is in agreement with the nonreactive mass and mixture-ratio distributions in that high performance is a result of the uniform mixture ratio exhibited by most of the injected mass.

The application of these data to the reacting system is not straightforward, since the reactions which constitute the combustion process may modify the mass and

mixture-ratio distributions measured with nonreacting liquids. For example, Elverum and Staudhammer, in Ref. 10, contend that liquid-phase reactions take place so rapidly in the $N_2O_4/N_2H_4$ propellant system that impinging streams are "blown apart" before the reaction has had an opportunity to proceed very far. However, another body of evidence (Refs. 11 and 12), which formed the basis for the design of this injector, indicates that this is not necessarily the case, and that information on nonreactive spray properties may be used to predict qualitative characteristics of the mass and mixture-ratio distributions of the reacting system (without denying that the reaction may modify the spatial qualities of these distributions as determined with nonreacting fluids). None of the available evidence indicates that these small streams "blow apart," and a high-speed movie showing the injector firing without a thrust chamber (i.e., as an "open flame," the condition under which Elverum and Staudhammer conducted their tests) clearly shows a mixture-ratio distribution which could only result from penetration of the propellant streams. Indications are that the role of liquid-phase reactions in determining spray properties in the $N_2O_4/N_2H_4$ system has not yet been clearly defined and that the scale of the jets and, perhaps, the jet velocity must be taken into consideration. In the present case, the orifice diameter was 0.020 in. (as against 0.070 in. in the experiment of Elverum and Staudhammer), and the average jet velocities were fairly high, both conditions favoring penetration of propellants. Since there does not appear to be any reason to doubt the applicability of the nonreacting-system data to the reacting system under discussion, a qualitative similarity between the data of Figs. 14 and 15 and the flow within the operating rocket engine is assumed.

### 2. Chamber Heat Flux

The circumferential distribution of heat flux to the combustion chamber wall was determined during short-duration uncooled-engine tests by using a transient thermocouple plug technique. Although it would have been desirable to measure heat flux to the wall at the nozzle throat, the small size of the nozzle used (0.75-in.-diameter throat) posed problems, both in fabricating a small enough thermocouple plug and in calculating heat fluxes under conditions where heat conduction would surely not be one-dimensional. Sufficient information was gathered, however, to allow extrapolation to the throat of the shape (i.e., relative local magnitude) of the heat-transfer distribution measured at the nozzle inlet.

The technique used to measure heat flux involved embedding a thermocouple in the wall of an uncooled combustion chamber, with the thermocouple junction at a known distance from the hot gas surface. An additional thermocouple was located on the outer wall. The time–temperature history of these two thermocouples, plus knowledge of the thermal properties of the wall material, allowed calculation of the temperature distribution in the wall between the two thermocouples. This distribution was then extrapolated to the hot gas surface, and the slope at the wall was used in the Fourier equation to obtain the heat flux. Since temperature gradients in the axial and circumferential directions are small relative to the temperature gradient through the wall, heat conduction along paths other than the radial path may be neglected without introducing appreciable error. Reference 13 explains the development and use of this transient technique.

The combustion chamber, which was fabricated to the geometry outlined in Table 1, was fitted with seven thermocouple plugs, as shown in Fig. 16. The chamber and the plugs were made of the same material (1020 steel) to reduce the possibility that the plug might cause a thermal gradient in the wall. The chromel–alumel thermocouple junctions were located 0.020 in. from the hot gas surface. By rotating the combustion chamber in relation to the injector in 10-deg increments between tests, it was possible to obtain a fairly complete map of local heat-transfer rates to the chamber wall.

Since the data were gathered during a series of tests, it was essential that those test conditions which influence heat transfer to the wall, such as chamber pressure and mixture ratio, be controlled from test to test, in order to ensure comparable results. In addition, the rocket engine starting transient was controlled by actuating both propellant valves with a timer to make certain that the thermal input to the wall prior to steady-state operation would be reproducible from test to test. These precautions ensured that the values of wall heat flux obtained during the series of tests were similar to those which would have been obtained in a single test, had it been possible to instrument the combustion chamber to the extent required. As an indication of the reproducibility of the test conditions, steady-state mixture ratio for the tests to be summarized was 1.003 to 1.041, with an arithmetic mean value of 1.018; steady-state chamber pressure was 150.2 to 152.0 psia, with an arithmetic mean of 151.0 psia. Experimental characteristic exhaust velocity $c^*$ was 5402 to 5569 fps, with an arithmetic mean of 5486 fps, or 94.3% of theoretical shifting equilibrium $c^*$. This variation of $\pm 1.5\%$ about the mean $c^*$ is indicative of the absolute precision of the instrumentation,

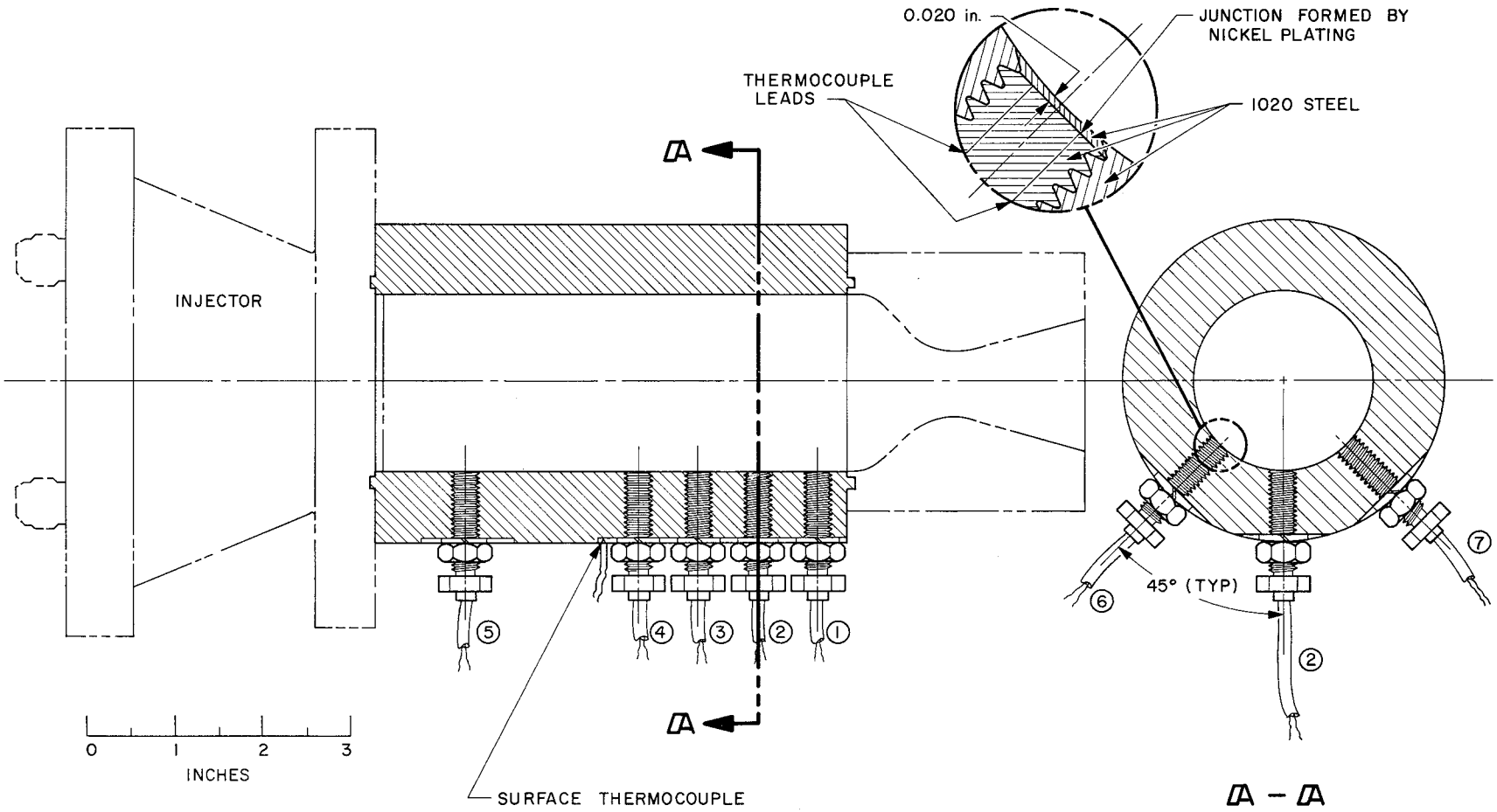


**Fig. 16. Combustion chamber, showing installation of transient thermocouple plugs**

since 93% of the tests fell within ±1.0% of the mean. Chamber pressure was measured at the injector face and was not corrected to nozzle-inlet conditions, nor was performance corrected for heat-transfer losses to the thrust chamber wall.

The circumferential distribution of chamber heat flux associated with the Mod II injector is shown in Fig. 17 for an axial location 1.0 in. upstream of the nozzle inlet at a time 4.80 sec after ignition. Chamber wall temperature was 400–600°F at this time, depending on location, and no attempt was made to normalize the heat flux to account for this variation. These data were obtained from the three thermocouples (Nos. 2, 6, and 7, as shown in Fig. 16) located 45 deg apart, resulting in three complete circumferential surveys as the chamber was rotated between tests. With the exception of the region between 30 and 70 deg, heat flux as determined by the three thermocouples was reproducible to ±9% in the worst case, with most of the readings reproducible to ±3%. The anomalous values between 30 and 70 deg cannot be explained at present; however, this lack of reproducibility appears to be a real effect associated with the injection–combustion system, rather than with the instrumentation. It will be noted that the nonreactive mixture-ratio distribution indicates that, in this region, mixture ratio is much higher than nominal.

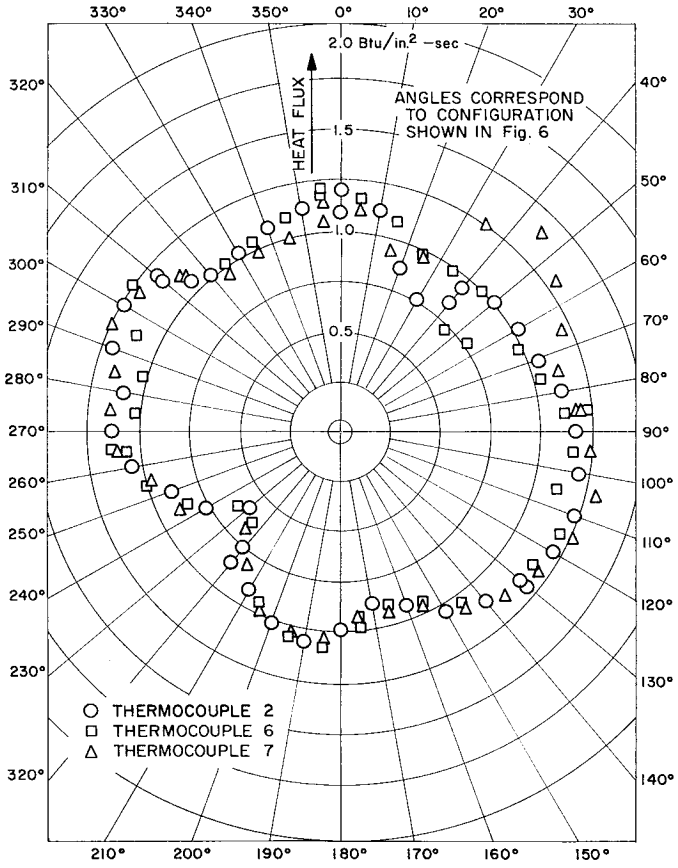


**Fig. 17. Circumferential distribution of heat flux produced by Mod II injector**

The circumferential heat-flux distributions obtained at thermocouples 1 and 3, respectively located 0.67 in. downstream and 0.67 in. upstream of thermocouple 2, show similar values and essentially the same shape as the distribution shown. This would indicate that those flow conditions which control the heat-transfer rate to the wall are well established at these stations, and the heat-flux distribution at the nozzle throat could be expected to show a similar shape. The distributions obtained from thermocouples 1 and 3 follow the distribution obtained from thermocouple 2 in the region between 30 and 70 deg, since these thermocouples are axially aligned, and values of heat flux at any angular location were determined for all three thermocouples during the same test.

Since simple boundary-layer relationships of the type developed in Ref. 5 suggest that convective heat flux may be determined principally by local flow rate per unit area near the wall, an attempt was made to relate local heat flux (Fig. 17) to local flow rate (Fig. 14). Although it would appear that, in some areas, heat flux may be *inversely* related to local flow rate (the opposite of the dependence normally assumed), no consistent correlation could be found. This is not to say that a relationship of this type does not exist; however, the nonreactive data obtained do not provide an adequate representation of flow rates at the wall (partly because the wall was omitted during the sampling tests). The possibility remains that a detailed study of conditions at the wall, using nonreactive techniques, could supply information relating to the convective transfer of heat to the wall.

The average heat flux measured at the nozzle inlet (i.e., thermocouple 1) was 0.99 Btu/in.²-sec at 4.80 sec. The average at a location 0.67 in. upstream (thermocouples 2, 6, and 7) was 1.03 Btu/in.²-sec, and, at 1.34 in. upstream (thermocouple 3), the average was 1.01 Btu/in.²-sec. These values were obtained by arithmetically averaging the heat flux measured at 10-deg increments around the circumference of the chamber; thus, they correspond to values that might be obtained from axially short circumferential water-cooled passages at some average wall temperature near 500°F. The average heat flux

over the downstream portion of the combustion chamber is thus seen to be essentially independent of axial location, with a value of 1.0 Btu/in.$^2$-sec. As a matter of interest, the heat flux at the nozzle inlet calculated by the method of Ref. 5 (and assuming a wall temperature of 500°F) is 1.14 Btu/in.$^2$-sec.

Additional information on the nature of the combustion-flow process produced by this injector was obtained by conducting a series of short-duration tests with uncooled steel combustion chambers. The combustion chamber was progressively shortened between tests, and the decrease in performance, as indicated by $c^*$, was noted. Results of the tests, shown in Fig. 18, indicate that, at chamber lengths longer than 2 in., no increase in $c^*$ was obtained. This would indicate that combustion was essentially completed within this volume, and further increases in performance due to mixing at longer lengths were counterbalanced by increased heat transfer to the longer chamber wall. As mentioned previously, this injector would be expected to produce a low level of secondary flow, so that mixture-ratio gradients should propagate axially along the chamber with very little mixing.

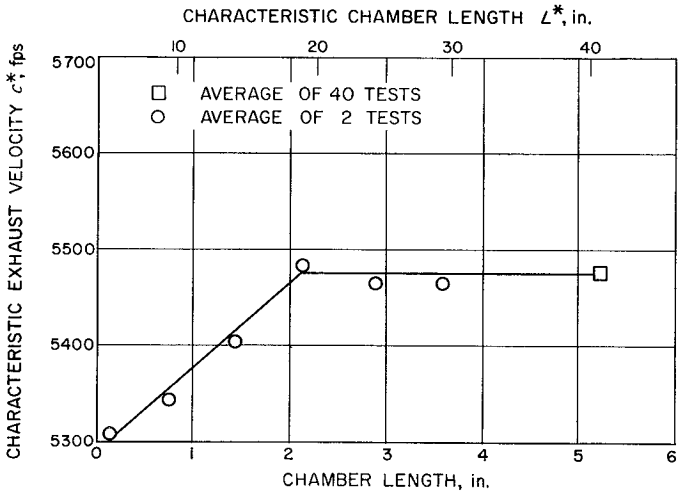


**Fig. 18. Effect of chamber length on characteristic exhaust velocity**

The data from these tests, plus the circumferential and axial heat-flux distributions obtained, indicate that combustion was completed and conditions near the wall established well upstream of the nozzle inlet. This suggests that an extrapolation of the shape of the circumferential heat-flux distribution from near the nozzle inlet to the throat may be made with a fair degree of confidence (except in the region between 30 and 70 deg, where the data were not reproducible). Thus, as mentioned above, the throat heat flux should resemble the shape shown in Fig. 17.

### 3. Effect on Materials

A cross section of the nozzle throat of the Refrasil–phenolic ablative thrust chamber tested for 30 sec with the Mod II injector is shown in Fig. 19. Erosion is seen to be nonuniform, ranging from a condition of no dimensional change in some areas to a rate as high as 5 mils/sec. It is interesting to note that this distribution of local erosion bears a relationship to the circumferential distribution of chamber heat flux shown in Fig. 17. For the most part, erosion occurred in regions of high heat flux to the chamber wall and did not occur in regions where chamber heat fluxes of less than 1 Btu/in.$^2$-sec were measured, indicating that the dimensional change was, in general, the result of a true thermal-ablation process. An exception to this is the region near 30 deg, where erosion rates of 1 to 2 mils/sec were observed, and where measured heat-transfer rates, although questionable, were generally less than 1 Btu/in.$^2$-sec. This is the region previously noted as being oxidizer-rich near the wall,

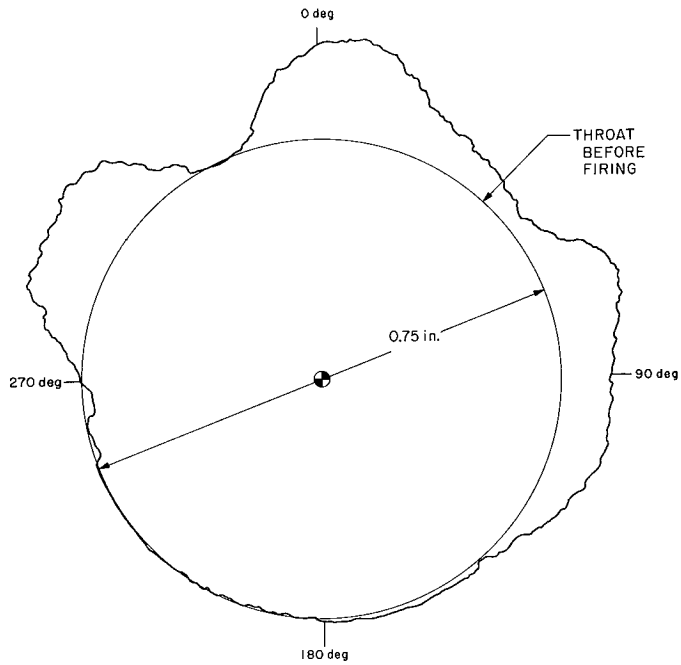


**Fig. 19. Cross section of nozzle throat of Refrasil–phenolic ablative thrust chamber after testing with Mod II injector**

indicating that reactions between oxygen in the products of combustion and the char would be possible in the absence of a melt layer. However, because the heat-flux data were not reproducible in this region, thus making an extrapolation to the throat hazardous, no firm conclusion can be drawn as to the relative influence of the thermal and chemical environments at this singular location.

Extrapolating the measured cold-wall heat flux to the throat by assuming the same dependence on geometry as that stated in the method of Ref. 5 and using an estimated wall temperature of 3500°F for the ablation of Refrasil, a maximum hot-wall throat heat flux of 1.1 Btu/in.$^2$-sec results. The maximum ablation rate thus corresponds to a heat of ablation of 3500 Btu/lb for this heat flux. This is in approximate agreement with data for steady-state ablation in the absence of chemical reaction of Refrasil–phenolic laminates (Ref. 14), indicating that only those regions of the throat which experienced the maximum heat flux underwent a steady-state ablation process. It is clear, then, as far as small engines are concerned, that steady-state ablation produces intolerable dimensional changes (of the order of 5 mils/sec or higher), and that methods of controlling the injection–combustion process to produce wall conditions which result in uniform transient or charring ablation in the throat are desirable.

Local erosion of both commercial and pyrolytic graphite throats, as shown in Fig. 20, can be related to the nonreactive mixture-ratio distribution shown in Fig. 15. Erosion of pyrolytic graphite, as illustrated in Fig. 20(a), occurred during 30-sec tests only in the region indicated by the nonreactive data to be oxidizer-rich near the thrust chamber wall. The maximum erosion of commercial graphite throats, as seen in Fig. 20(b), also occurred in this region, indicating that oxygen contained in the products of combustion of this high-mixture-ratio region produced rapid oxidation of both types of graphite. Equilibrium thermochemical calculations show that the products of combustion of $N_2O_4/N_2H_4$ contain 8% (by volume) oxygen at a mixture ratio of 2.0, although, at the nominal mixture ratio of 1.0, practically no free oxygen is present.

These results demonstrate that the local conditions within the thrust chamber, as determined by the injector, affect the local performance of thrust chamber materials. However, some of these effects may be rather less obvious than the asymmetric erosion observed. For example, the failure of the tungsten thrust chamber shown in Fig. 11 occurred at the center of the cold streak observed in the circumferential distribution of heat flux (i.e., at a chamber angle of 230 deg). Thermal expansion of the thrust chamber in the radial direction would be expected to introduce a bending stress in the cold por-

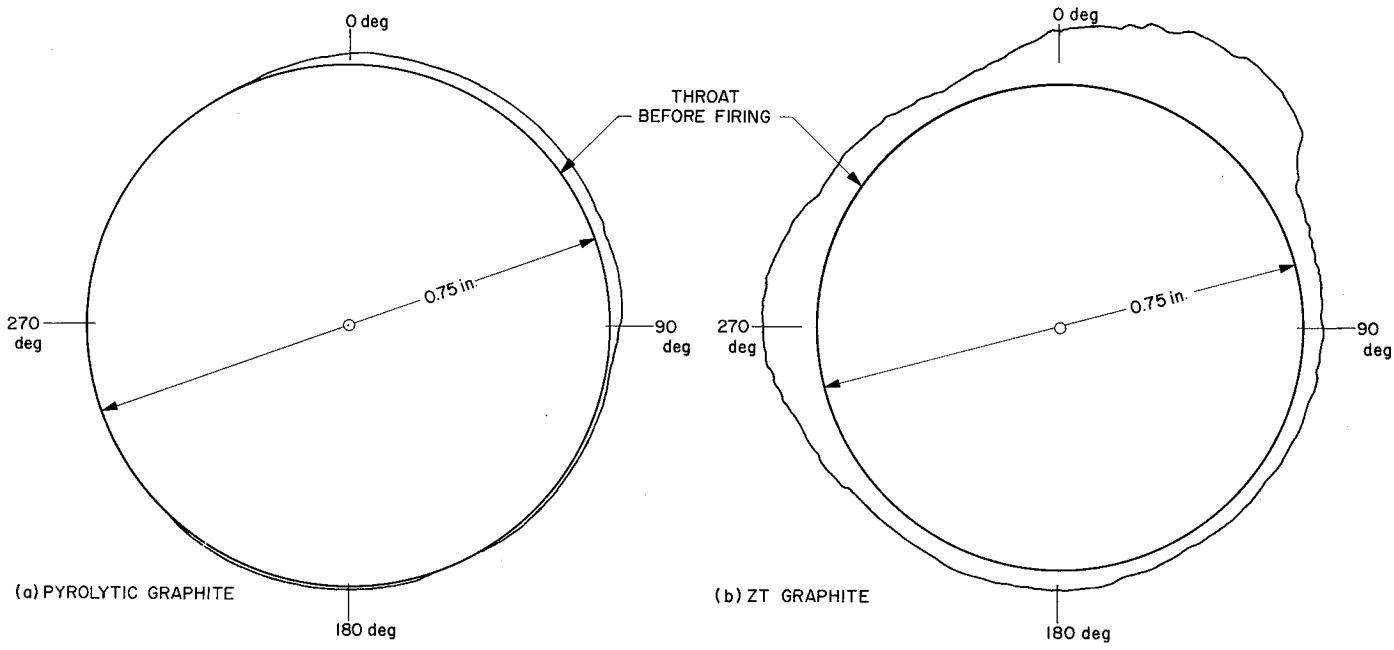


**Fig. 20. Cross section of nozzle throats of pyrolytic and commercial graphite thrust chambers after testing with Mod II injector**

tion, with the inner surface in tension. Since the inner surface was quite rough, and the wall temperature at the center of the cold streak may have been below the brittle–ductile transition point at the time failure occurred, the crack could easily have resulted from stress concentrations introduced by the rough wall and amplified by the brittle nature of tungsten. This failure, then, although at first glance random in nature, was probably injector-related. Similarly, nonuniform wall temperatures resulting from injector nonuniformities could have contributed to failure of the two freestanding pyrolytic graphite thrust chambers tested.

## V. CONCLUSIONS

Local erosion of uncooled thrust chamber materials is determined by the local thermal and chemical environments at the thrust chamber wall and by the thermal and chemical properties of the wall material. Local gas-side boundary conditions are only casually related to gross rocket engine system characteristics, such as equilibrium gas temperature, nominal mixture ratio, and average mass flow rate, since nonuniformities in the injection–combustion process may dominate conditions near the wall.

An approximation to the mass and mixture-ratio distributions produced by an impinging-stream injector can be obtained by substituting nonreacting liquids for the injected propellants and sampling the spray produced. Provided that the method of injection can be controlled to ensure that stable, reproducible liquid streams (and hence, a reproducible spray) are formed, the spray properties deduced from such nonreacting tests may be used for qualitative explanations of chemically induced erosion of thrust chamber wall materials.

The distribution of heat flux to the thrust chamber wall may be calculated by use of temperature measurements taken from embedded thermocouples during short-duration tests. The local thermal environment indicated by such measurements may be related to thermally induced phenomena, such as ablation and thermal stresses, which affect the performance of uncooled thrust chamber materials.

Refrasil–phenolic ablative plastics are suitable for use in small bipropellant engines, provided that the thermal input to the wall can be made low enough to allow the plastic to behave as a charring ablator. An alternative is a nonablating insert in high-heat-flux regions such as the throat. Pyrolytic graphite and tungsten are also suitable for use in small bipropellant engines, provided that the difficulties introduced by the brittle nature of both materials can be overcome. These difficulties arise during both fabrication and firing, when thermal gradients can produce failures of the "thermal-shock" variety. Local oxidation of both materials is a problem amenable to attack from two directions:

1. Development of suitable coatings.
2. Control of gas composition near the wall by proper control of the injected propellants.

## REFERENCES


1. Kotlensky, W. V., and Martens, H. E., *Tensile Properties of Pyrolytic Graphite to 5000°F,* Technical Report No. 37-71, Jet Propulsion Laboratory, Pasadena, March 10, 1961.

2. Powell, W. B., Irving, J. P., and Guenther, M. E., *Chlorine Trifluoride–Hydrazine Liquid Propellant Evaluation and Rocket Motor Development,* Technical Report No. 32-305, Jet Propulsion Laboratory, Pasadena, May 15, 1963.

3. Rupe, J. H., "Bridging the Gap Between Injector Hydraulics and Combustion Phenomena in Liquid Propellant Rocket Engines," *Bulletin of the First Meeting of the Joint Army-Navy-Air Force Liquid Propellant Group, Volume III,* November 1959, pp. 335–360 (Confidential).

4. Rupe, J. H., *On the Dynamic Characteristics of Free-Liquid Jets and a Partial Correlation with Orifice Geometry,* Technical Report No. 32-207, Jet Propulsion Laboratory, Pasadena, January 15, 1962.

5. Bartz, D. R., "A Simple Equation for Rapid Estimation of Rocket Nozzle Convective Heat Transfer Coefficients," *Jet Propulsion,* January 1957, pp. 49–51.

6. Stephanou, S. E., Oliver, R. C., Baier, R., and Getz, R., *Chemical Corrosion of Rocket Liner Materials and Propellant Performance Studies,* First Quarterly Technical Summary Report, Aeronutronic Division, Ford Motor Company, Newport Beach, California, September 15, 1962.

7. Levy, M., *Oxidation of Pyrolytic Graphite Between 1250°F and 1850°F,* Technical Report No. WAL TR 851.4/1, Watertown Arsenal Laboratories, Watertown, Massachusetts, May 1961.

8. Sumida, W. K., and Baskin, Y., *Study of the Mechanism of Failure of Rocket Materials and Materials Research,* Quarterly Report No. 2, Armour Research Foundation, Chicago, Illinois, January 3, 1961.

9. Rupe, J. H., *The Liquid Phase Mixing of a Pair of Impinging Streams,* Progress Report No. 20-195, Jet Propulsion Laboratory, Pasadena, August 6, 1953.

10. Elverum, G. W., Jr., and Staudhammer, P., *The Effect of Rapid Liquid-Phase Reactions on Injector Design and Combustion in Rocket Motors,* Progress Report No. 30-4, Jet Propulsion Laboratory, Pasadena, August 25, 1959.

11. *Research Summary No. 36-2, Vol. I, Part Two,* Jet Propulsion Laboratory, Pasadena, April 15, 1960, pp. 28–31.

12. *Research Summary No. 36-6, Vol. II,* Jet Propulsion Laboratory, Pasadena, January 2, 1961, pp. 45–46.

13. Powell, W. B., Howell, G. W., and Irving, J. P., *A Method for the Determination of Local Transient Heat Flux in Uncooled Rocket Motors,* Technical Report No. 32-257, Jet Propulsion Laboratory, Pasadena, July 1, 1962.

14. Adams, M. C., "Recent Advances in Ablation," *ARS Journal,* September 1959, pp. 625–632.